Electrochemical Assembly of a CdS Semiconductor Nanoparticle Monolayer on Surfaces: Structural Properties and Photoelectrochemical Applications

Eran Granot, Fernando Patolsky, and Itamar Willner*

Institute of Chemistry, The Farkas Center for Light-Induced Processes, The Hebrew University of Jerusalem, Jerusalem 91904, Israel

Received: December 24, 2003; In Final Form: February 17, 2004

p-Aminothiophenol-capped CdS nanoparticles (8.5 ± 0.3 nm) were assembled as a monolayer by their electropolymerization into a *p*-aminothiophenol-monolayer-functionalized Au electrode. The resulting CdS nanoparticle monolayer, 9.0×10^{11} particles/cm^2, was characterized by AFM, XPS, and microgravimetric quartz crystal microbalance measurements. The dianiline-bridged CdS nanoparticles assembled on the Au electrode revealed highly efficient photoelectrochemical properties in the presence of triethanolamine as sacrificial electron donor. The dianiline bridging unit was found to have an important function in the photocurrent generation. At an applied potential that is more positive than −0.1 V, the dianiline exists in its oxidized state, and it acts as an electron relay that mediates electron transfer from the semiconductor to the bulk electrode. The quantum yield at an applied potential of 0.4 V corresponds to $\phi = 5.7\%$. At an applied potential of less than −0.1 V the polymer exists in its reduced state, and under these conditions the dianiline units act as a tunneling medium for transporting the electrons from the semiconductor nanoparticles to the electrode.

Introduction

The unique electronic,[1] photonic,[2] and catalytic[3] properties of metal or semiconductor particles are of great interest for the fabrication of nanoscale devices.[4,5] The organization of nanoparticles as functional devices requires their assembly on surfaces. Extensive research efforts are directed in recent years to the assembly of 2D and 3D metal or semiconductor nanostructures on surfaces, and several review articles have addressed this topic.[6] Covalent attachment of nanoparticles to surfaces[7] or electrostatic attraction of nanoparticles to modified surfaces[8] was used to prepare 2D particle arrays. Similarly, the covalent linking or cross-linking[9] of nanoparticles was used to prepare 3D nanoparticle structures in addition to the electrostatic layer-by-layer deposition of nanoparticles on surfaces using molecular[10] or macromolecular[11] cross-linkers, or the organization of layered nanoparticle structures using molecular[12] or biomolecular[13] cross-linkers. Incorporation of nanoparticles into polymer matrixes was also reported as a means to generate thin nanoparticle/polymer films on surfaces.[14] Electropolymerization of polymerizable monomers is a general method to assemble polymer films on electrode surfaces, and the electropolymerization of monomer-functionalized metal nanoparticles, for example, pyrrole-capped Au nanoparticles,[15] was reported to yield a 2D nanoparticle array.

Tailoring of semiconductor nanostructures on electrode supports has attracted substantial research effort directed to the development of solar cells[16] and optoelectronic[17] and photonic[18] devices. The assembly of nanoporous semiconductor particles on surfaces and the immobilization of dyes on the roughened semiconductor surfaces was reported as an effective interface for photosensitization of the semiconductor and for the efficient generation of photocurrents.[19] An intrinsic limitation of semiconductor nanoparticles in photoelectrochemical applications is the rapid electron−hole recombination. At the molecular level, triads consisting of donor−photosensitizer−electron acceptor monolayers associated with electrodes were reported as organized assemblies for enhanced photocurrent generation.[20] Photoinduced vectorial electron transfer in the systems leads to the spatial separation of the redox products and their stabilization against recombination. This concept for stabilization of the photogenerated redox species was also adopted in semiconductor nanoparticle systems. Photoinduced vectorial electron transfer in a hybrid nanoparticle system was reported to retard the electron−hole recombination.[21] Similarly, photosensitized core shell nanoparticle systems on electrodes were reported as organized matrixes for effective charge separation and enhanced photocurrent generation.[22]

Here we wish to report on the preparation of *p*-mercaptoaniline-capped CdS nanoparticles, their electropolymerization on a Au electrode in a monolayer assembly, and the application of the resulting array for photocurrent generation.

Experimental Section

Materials. Sodium sulfide ($Na_2S \cdot 9H_2O$, 98%) and *n*-heptane <99% were purchased from Sigma. Cadmium perchlorate hydrate ($Cd(ClO_4)_2 \cdot xH_2O$), dioctyl sulfusuccinate sodium salt 96%, 2-mercaptoethane sulfonic acid sodium salt 98%, and triethanolamine hydrochloride >99% were purchased from Aldrich. *p*-Aminothiophenol *p*-ATP (>90%) was purchased from Fluka. All other materials were purchased from Aldrich and used as received without further purification.

Borosilicate glass slides coated with a thin Cr sublayer (2.5 ± 1.5 nm) and a polycrystalline Au layer (250 ± 50 nm) were used as electrodes in all experiments (supplied by Arandee, Germany).

Methods. Absorption spectra were recorded on a Uvikon 860 (Kontron) spectrometer. Cyclic voltammetry was performed in

* To whom all correspondence should be addressed. Phone: 972-2-6585272. Fax: 972-2-6527715. E-mail: willnea@vms.huji.ac.il.

10.1021/jp038004o CCC: $27.50
Published on Web 04/15/2004

a standard electrochemical cell using the functionalized Au electrode. A conventional three-electrode cell, consisting of the Au electrode, a glassy carbon auxiliary electrode isolated by a glass frit, and a saturated calomel electrode (SCE) connected to the working volume with a luggin capillary, was used for the electrochemical measurements. The potential measured with cyclic voltammetry is reported versus SCE. The cell was positioned in a grounded Faraday cage. The electrochemical experiments were performed with a potentiostat (EG&G, model 283) connected to the computer (EG&G Software Power Suite 103). The electrochemical measurements were performed in 0.1 M phosphate buffer, pH = 7.5, as background electrolyte. Atomic force microscopy (AFM) images were acquired in tapping mode in air by a Smena B instrument (NT-MDT, Russia) with a 30 μm scanner and NSC-16 cantilever (resonance frequency 180 kHz). The scan rates used were 1.5−2.5 Hz with a cantilever oscillation amplitude of the order of 20−40 nm.

Microgravimetric quartz crystal microbalance (QCM) measurements were performed with a home-built instrument linked to a frequency analyzer (Fluke) using Au−quartz crystals (AT-cut 10 MHz). The geometrical area of the Au electrode was 0.2 ± 0.05 cm^2, roughness 3.5. Prior to each measurement the modified QCM crystals were dried under a flow of argon, and the crystal frequencies were determined in air. The surface coverage of the respective component was determined by following the frequency change of the crystals upon the stepwise assembly of the different component. The surface coverage was estimated using the Sauerbrey equation, (eq 1), where Δm is the mass change, f_o is the resonance frequency of the quartz crystal, A is the piezoelectrically active area, ρ_q is the density of the quartz (2.648 g cm^{-3}), and μ_q is the shear modulus (2.947×10^{11} dyn cm^{-3}) for AT-cut quartz.

$$\Delta f = -2f_o^2 \Delta m/A(\mu_q \rho_q)^{1/2} \quad (1)$$

Photoelectrochemical experiments were performed using a home-built photoelectrochemical system that included a 300W Xe lamp (Oriel, model 6258) as the light source, a monochromator (Oriel, model 74000, 2 nm resolution), and a chopper (Oriel, model 76994). The electrical output from the cell was sampled by a lock-in amplifier (Stanford Research model SR 830 DSP). The shutter chopping frequency was controlled by a Stanford Research pulse/delay generator model DE 535. The photoelectrode consisted of the Au electrode modified with the cross-linked mercaptoaniline-capped CdS nanoparticles (working electrode). A graphite electrode was used as a counter electrode. The photogenerated current was measured between the working and the counter electrode. The electrolyte solution consisted of 20 mM triethanolamine (TEA) in 0.1 M phosphate buffer, pH = 11.5. The Au electrode, prior to modification, and after modification, was placed in the photoelectrochemical cell. A current meter was positioned between the two electrodes. The difference of the measured current that reached the current meter was assumed to correspond to the amount of aniline−CdS nanoparticles absorbed on the electrode.

In some experiments we used a three-electrode cell configuration for measuring the photocurrent at different applied potentials. In these experiments a saturated calomel electrode (SCE) was introduced as the reference electrode.

XPS analyses were performed with a Kratos AXIS-HS spectrometer, using a monochromatized Al Kα source. Scans were usually run at 45 or 75 W. All data acquisitions were performed in a hybrid mode (using electrostatic and magnetic lenses) and detection pass energies of 40−80 eV. All XPS measurements were carried out at room temperature, under vacuum conditions of $1.0-3.0 \times 10^{-9}$ Torr. All spectra were acquired with an electron flood gun for charge neutralization. The spectrometer energy scale was routinely calibrated according to the ISO TC/201 SC7 international procedure for binding energy (BE) Au $4f_{7/2}$ = 83.98 and Cu $2p_{3/2}$ = 932.67. Data processing was done with VISION 2.1 software (Kratos).

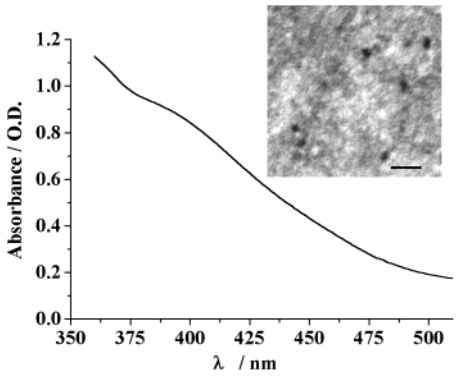

Figure 1. Absorption spectrum of the *p*-aminothiophenol/mercaptoethane sulfonic acid capped CdS nanoparticles (8.5 ± 0.3 nm). Inset: TEM image of the CdS nanoparticles, scale bar 30 nm.

Preparation of CdS Nanoparticles.[23] An AOT/*n*-heptane water-in-oil microemulsion was prepared by the solubilization of 3.5 mL of distilled water in 100 mL of *n*-heptane in the presence of 7.0 g of the AOT surfactant (dioctyl sulfosuccinate sodium salt). The resulting mixture was separated into 60 mL and 40 mL of reverse-micelle subvolumes. Aqueous solutions of $Cd(ClO_4)_2$ (240 μL, 1.35 M) and Na_2S (160 μL, 1.33 M) were added to the 60 mL and 40 mL subvolumes, respectively, and the two solutions were mixed and stirred for 1h to yield the CdS nanoparticles. For the preparation of thiol-capped CdS nanoparticles, a mixture consisting of an aqueous solution of 2-mercaptoethane sulfonic acid sodium salt (330 μL, 0.32 M) and *p*-aminothiophenol in ethanol (66 μL, 0.32 M) was added to the resulting micellar solution and the mixture was stirred for 14 h under argon. Pyridine, 20 mL, was added to the solution, and the resulting precipitate was centrifuged and washed with *n*-heptane, petroleum ether, butanol, and methanol.

Modification of Au Electrodes. Gold surfaces were treated with piranha solution (70% sulfuric acid and 30% hydrogen peroxide) for a period of 30 s and washed thoroughly with distilled water and absolute ethanol. The resulting gold electrodes were modified with *p*-aminothiophenol (*p*-ATP), 50 mM in ethanol, for a period of 24 h.

Assembly of the CdS Nanoparticle Monolayer. The *p*-aminothiophenol-modified gold surfaces were subjected to electrochemical scans in the presence of 0.1 M phosphate buffer, pH = 7.5, containing 1 mg/mL of CdS nanoparticles. Voltage range: −0.5 to +0.5 V versus SCE. Scan rate: 100 mV/sec.

Results and Discussion

The CdS nanoparticles were prepared according to the reverse-micelle method,[23] and the resulting particles were capped with a mixed mercaptoethane sulfonate/*p*-aminothiophenol monolayer. The sulfonate units are added to the capping layer in order to allow the solubilization of the particles in an aqueous medium. The resulting particles were characterized by TEM, Figure 1, inset, and they reveal a narrow size distribution, diameter 8.5 ± 0.3 nm. By the elementary analysis of the capping layer associated with a known amount of particles, we estimate the ratio of the mercaptoethane sulfonate/*p*-aminothiophenol in the protecting layer to be 7:1 (although the modifying solution includes a ratio of 5:1). The absorbance

SCHEME 1: (A) Electrochemical Assembly of the *p*-ATP/Mercaptoethane Sulfonic Acid Functionalized CdS Nanoparticle Monolayer on a *p*-ATP-Monolayer-Modified Au Electrode and (B) Reversible Redox Processes of the *p*-ATP-Dimer-Functionalized CdS Nanoparticles Associated with the Electrode

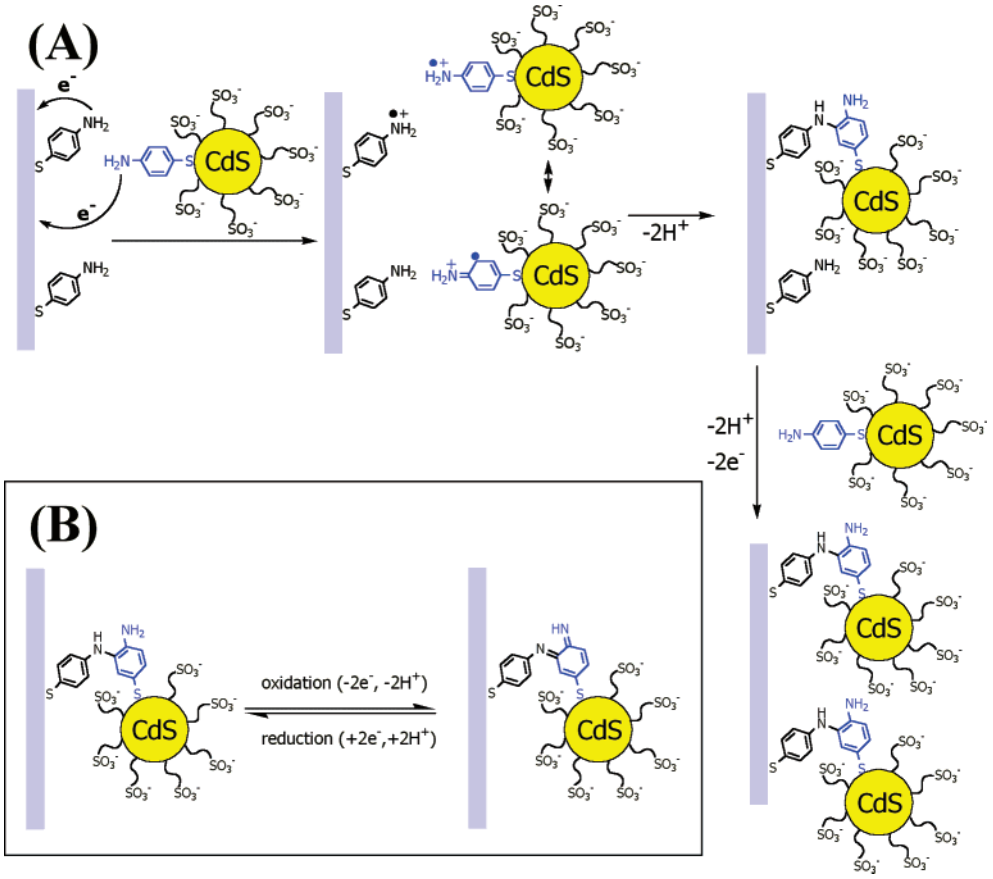

spectrum of the particles is depicted in Figure 1. It shows a shoulder at about 400 nm.

The *p*-aminothiophenol-functionalized CdS nanoparticles were electrochemically attached to a Au surface, premodified with a *p*-aminothiophenol monolayer used as a glue layer for the binding of the CdS nanoparticles, Scheme 1A. The deposition of the particles on the surface was accomplished by the repetitive application of potential cycles from −0.5 to +0.5 V versus SCE on the electrode. We find that after about 70 cycles, the coverage of the electrode by the nanoparticles reaches saturation (for the characterization of the time-dependent buildup of the nanoparticle monolayer, vide infra). Figure 2 shows the cyclic voltammogram of the resulting molecularly cross-linked CdS-nanoparticle-functionalized electrode after completion of the electropolymerization process, washing off of the solution that contained the modified particles, and substitution of the electrolyte solution with a phosphate buffer solution. The cyclic voltammogram shows two quasi-reversible redox waves: One redox couple, centered at about 0.10 V versus SCE (E_{ox} = 0.145 V vs SCE; E_{red} = 0.04 V vs SCE), is attributed to the redox response of the bisaniline cross-linking units. The second redox wave centered at about −0.30 V versus SCE (E_{ox} = −0.20 V vs SCE; E_{red} = −0.36 V vs SCE) is attributed to Cd^{2+} ions linked to the CdS surface. The electrochemical response of CdS nanoparticles was previously reported.[24] Although the electrical response corresponding to the Cd^{2+} ions is pH-independent, the redox wave that corresponds to the cross-linking units is pH-dependent, Figure 2, inset. The observed potential changes as a function of pH, slope 30 mV·pH^{-1} are consistent with a $2e^-$ oxidation process, Scheme 1B. It should be noted that polyaniline is redox-inactive at neutral pH solutions, and

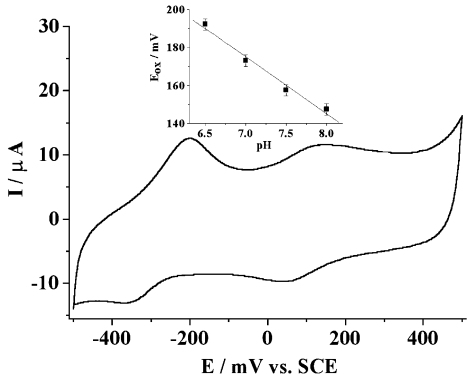

Figure 2. Cyclic voltammogram corresponding to the electrochemically generated cross-linked CdS nanoparticle monolayer on a Au electrode. The electrolyte solution consists of 0.1 M phosphate buffer, pH 7.5, scan rate 100 mV s^{-1}, under Ar. Inset: Peak potentials for the oxidation of the aniline-dimer cross-linking units as a function of different pH values.

similarly, a *p*-aminothiophenol monolayer assembled on a Au electrode reveals redox activity only in acidic pH media.[25] It was shown, however, that the doping of polyaniline with negatively charged sulfonate units,[26] or the incorporation of negatively charged poly(acrylic acid)[27] or DNA[28] units, yields a redox-active polymer at neutral and even basic aqueous solutions. Although the mechanism of the redox activation of polyaniline by the anionic dopants is not fully understood, we assume that the sulfonate functionalities associated with the CdS nanoparticles provide the anionic doping that activates the redox functions of the aniline dimer at neutral and even slightly basic aqueous solutions.

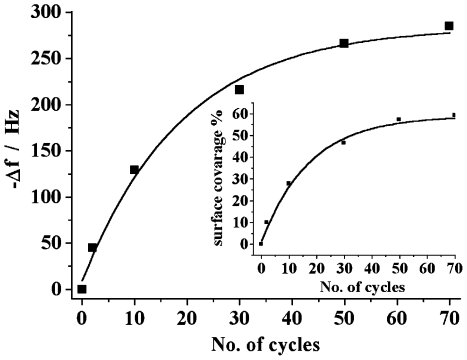

Figure 3. Frequency changes of the Au−quartz crystal upon the electrochemical coupling of the CdS nanoparticles on the *p*-ATP-monolayer-functionalized crystal. Inset: Surface coverage of the CdS nanoparticles on the crystal as derived from the respective experimental frequency changes.

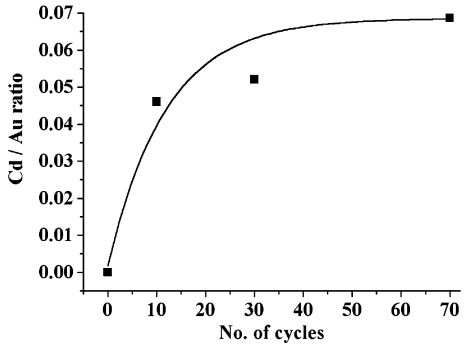

Figure 4. Cd/Au ratio on a Au electrode upon the time-dependent electrochemical coupling of the nanoparticles on the surface. The Cd/Au ratio was determined by XPS analyses.

The cross-linked CdS nanoparticle interface generated on the Au surface was characterized by microgravimetric quartz crystal microbalance (QCM) measurements, X-ray photoelectron spectroscopy (XPS) analyses, and AFM imaging. Figure 3 shows the frequency changes of a *p*-aminothiophenol-modified Au−quartz crystal upon the electrochemically induced attachment of the CdS nanoparticles by cycling the potential on the electrode. After about 70 cycles, the crystal frequency decreases by about 300 Hz, and it levels off to a constant value. The decrease of the crystal frequency implies the accumulation of a mass on the surface. The frequency changes associated with the Au−quartz crystal upon the electrochemical attachment of the CdS particles was translated to mass changes occurring on the crystal (using the Sauerbrey equation) and to the surface coverage of the CdS nanoparticles, Figure 3, inset, assuming that the weight of the CdS nanoparticle is about $1.5 \cdot 10^{-18}$ g/particle. Knowing the diameter of the CdS nanoparticles (8.5 $\pm$ 0.3 nm), an experimental surface coverage of about 9.0×10^{11} particles/cm^2 was calculated, which corresponds to about 60% of a densely packed CdS nanoparticle monolayer. Theoretical predictions suggest that a random densely packed monolayer of spherical objects will reveal about 65% surface coverage of the theoretical coverage of a dense monolayer.[29] Thus, the QCM experiments suggest that a random densely packed monolayer of the CdS nanoparticles is generated on the Au surface. (The ordered densely packed monolayer originates from the sequential 2D dense ordering of the nanoparticles around a single clustering site throughout the entire surface. The random 2D packing of the nanoparticle layer originates from the close-packed ordering of the nanoparticles around randomly distributed nanoparticle clustering sites.) Figure 4 shows the Cd/Au element ratio on the Au electrode upon the buildup of the nanoparticle monolayer, as derived from XPS measurements, after correction for ionization cross section variations. The Cd content associated with the interface increases as the number of applied potential cycles increases, and it levels off to a constant value after about 70 cycles, consistent with the electrochemical and QCM experiments. This suggests the completion of the CdS nanoparticle monolayer assembly after about 70 electrochemical cycles.

A nice direct confirmation of the electrochemically induced formation of the CdS nanoparticle monolayer on the Au surface is obtained by the AFM imaging of the interface. Figure 5 shows the AFM images of the surface upon the application of different numbers of electrochemical cycles for generating the nanoparticle monolayer. The application of the first two electrochemical cycles yields the deposition of a few CdS nanoparticles on the surface, Figure 5B. Clearly, increasing the number of applied potential cycles results in a higher surface coverage of nanoparticles, and after 70 cycles the surface is saturated with the CdS nanoparticle monolayer, Figure 5D. The height of the particles extracted from the AFM measurements is consistent with the dimensions found by TEM. The analysis of the electrochemically induced assembly of the particles on the surface indicates that a dense 2D monolayer of CdS nanoparticles is formed without an extension into a 3D configuration. This is explained by the cross-linked dimerization between the *p*-aminothiophenol monomer units linked to the Au surface and to the CdS nanoparticles. Once the dimers are formed, Scheme 1A, the subsequent dimerization of free polymerizable monomers units on the surface of the attached nanoparticles with solution-solubilized particles (interparticle dimerization or particle polymerization), is blocked because the particles on the surface act as insulating sites.

The Au electrode, functionalized with CdS nanoparticles, was employed as an active interface for the generation of photocurrents. Figure 6A shows the photocurrent spectra of the CdS-nanoparticle-modified Au surfaces that were generated by treatment with a different number of applied potential cycles in the presence of CdS nanoparticles. That is, the functionalized electrodes differ in the surface coverage of the CdS particles on the respective surfaces. The photocurrent measurements are performed in the presence of triethanolamine (TEA) as a sacrificial electron donor. As the surface coverage of the CdS nanoparticles on the surface increases, the photocurrent signal is enhanced. The photocurrent intensities reach a saturation value after about 70 electropolymerization cycles, Figure 6A inset, consistent with the formation of a dense monolayer of the CdS nanoparticles. Figure 6B compares the photocurrent action spectrum of the saturated, surface-cross-linked CdS nanoparticle monolayer, curve a, with that observed for the electropolymerized *p*-ATP monolayer associated with the Au surface in the absence of CdS nanoparticles, curve b. Only the system that includes the CdS nanoparticles generates the photocurrent. A further control experiment indicates that a high stable photocurrent is generated only in the presence of TEA. These results enable us to define the sequential steps that lead to the formation of the photocurrent in the system. Photoexcitation of the semiconductor nanoparticles leads to the formation of an electron−hole pair. In the absence of the electron donor, rapid electron−hole recombination prevents the formation of a steady-state current in the system. In the presence of the sacrificial electron donor triethanolamine (TEA), the scavenging of the valence-band holes prevents the electron−hole recombination and this allows the formation of the photocurrent. It should be noted that the photocurrent action spectra of the surface-bound

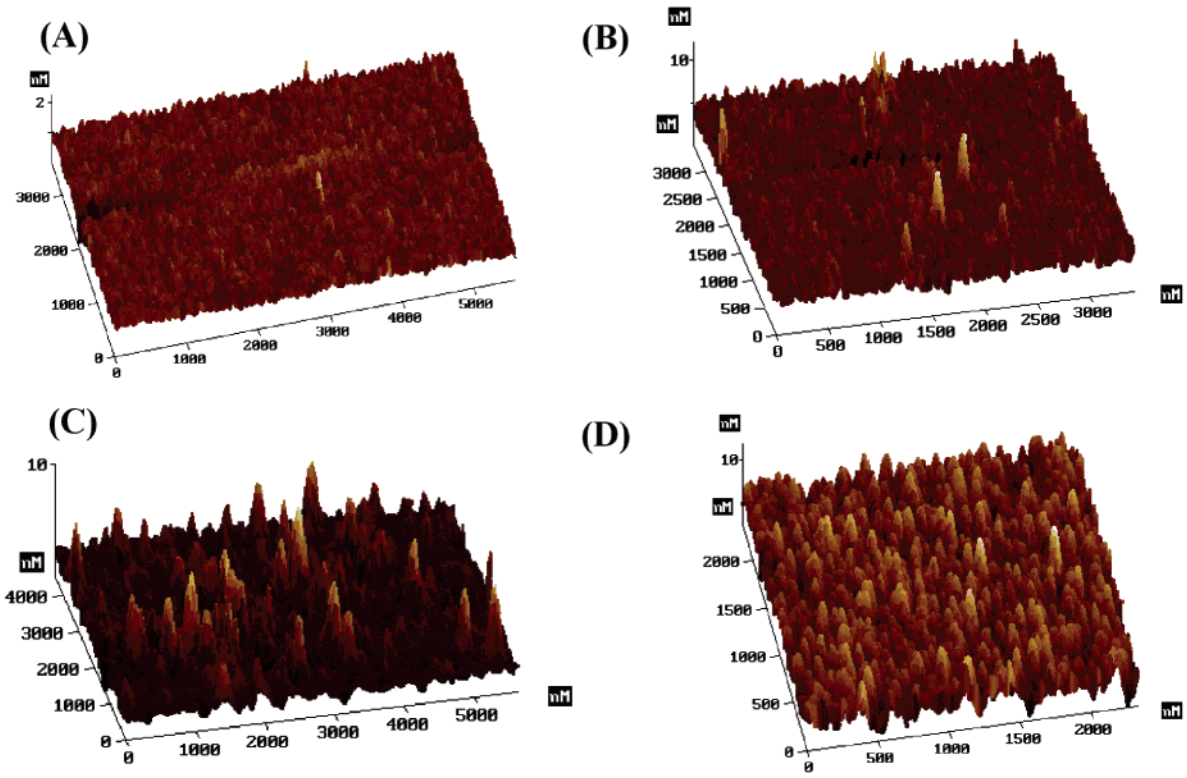

Figure 5. AFM images of (A) the *p*-ATP-modified Au surface and (B, C, and D) after the electrochemically induced linkage of the functionalized nanoparticles by 2, 10, and 70 electrochemical cycles, respectively.

CdS nanoparticles does not fully overlap with the absorption spectrum of the CdS nanoparticles. We find in the photocurrent action spectra a shoulder at about 440 nm that corresponds to a 40 nm shift as compared to the absorption spectrum of the CdS nanoparticles in solution. Although this phenomenon is not fully understood by us, we suggest that the surface-confined electropolymerization of the CdS nanoparticles by the *p*-aminothiophenol units leads to the formation of new surface traps for the conduction-band electrons. This lower-energy-lying surface state may then lead to the shift in the photocurrent action spectra. It should be noted that an onset in the photocurrent is already visible at 500 nm, a wavelength at which the absorbance of the nanoparticles is negligible. This might suggest that upon the polymerization of the CdS particles on the electrode, new surface states, and particularly electronic coupling between the aniline dimer and the semiconductor particles, are generated. Note that the photocurrent measurements are performed at pH = 11.5. The basic pH (pH > 8.5) of the medium is required to keep the TEA electron donor in its nonprotonated state. We find, however, that an aqueous medium of higher basicity yields improved photocurrent yields. This presumably originates from the formation of $Cd^{+}-OH$ traps on the nanoparticle surface that facilitates charge separation and photocurrent formation. Accordingly, all photocurrent measurements were performed at pH = 11.5.

Figure 7, curve a, shows the effect of applied potential on the resulting photocurrent intensities at $\lambda = 440$ nm. We observe a non-monotonic increase in the photocurrent intensity upon the biasing of the potential on the electrode to more positive values. We observe a decrease in the photocurrent upon changing the applied potential from +0.4 V to about −0.10 V vs SCE. From that potential a sharp decrease in the photocurrent is observed upon biasing of the potential to more negative values, and at −0.30 V the photocurrent is fully blocked. At pH = 11.5, the pH at which the photocurrent measurements are performed, the cross-linking aniline dimers exist in the oxidized form up to about −0.10 V versus SCE, whereas their reduced form is generated at more negative potentials. Thus, the enhanced photocurrents in the presence of the oxidized dimers suggest that the dimers participate in the transport of conduction-band electrons to the electrode. That is, in the oxidized state the dianiline cross-linking units act as electron acceptors that trap the conduction-band electrons. As the potential on the electrode retains the bridging units in their oxidized form, the trapped electrons are transferred to the electrode. This leads to effective charge transport that retards the electron−hole recombination and yields improved photocurrents. At potentials that are more negative than −0.10 V, the cross-linking dimers exist in their reduced state. This turns the cross-linking units into a tunneling medium for the conduction-band electrons that lack mediating electron transfer properties. Biasing the electrode potential to negative values sharply decreases the photocurrent. This is consistent with the fact that as the potential on the electrode is more negative, the ejection of the conduction-band electrons is less favored, resulting in the effective electron−hole recombination and the blockage of the photocurrent. The importance of the oxidized dianiline bridging units in the electron-transfer-mediated generation of the photocurrent is further emphasized by comparing our system to a CdS monolayer assembly that is covalently linked to the electrode by redox-inactive bridging units. In the reference system CdS nanoparticles stabilized by a cystamine/mercaptoethane sulfonic acid capping mixed monolayer were covalently linked to a Au electrode functionalized with a cysteic acid monolayer. The maximum photocurrent in this system in the presence of triethanolamine, pH = 11.5, corresponds to 66 nA, Figure 7, curve b. The *p*-aminothiophenol CdS nanoparticle cross-linked monolayer reveals several differences when compared to the cysteic acid−cystamine covalently coupled CdS nanoparticle system: (i) The voltage-dependent photocurrent

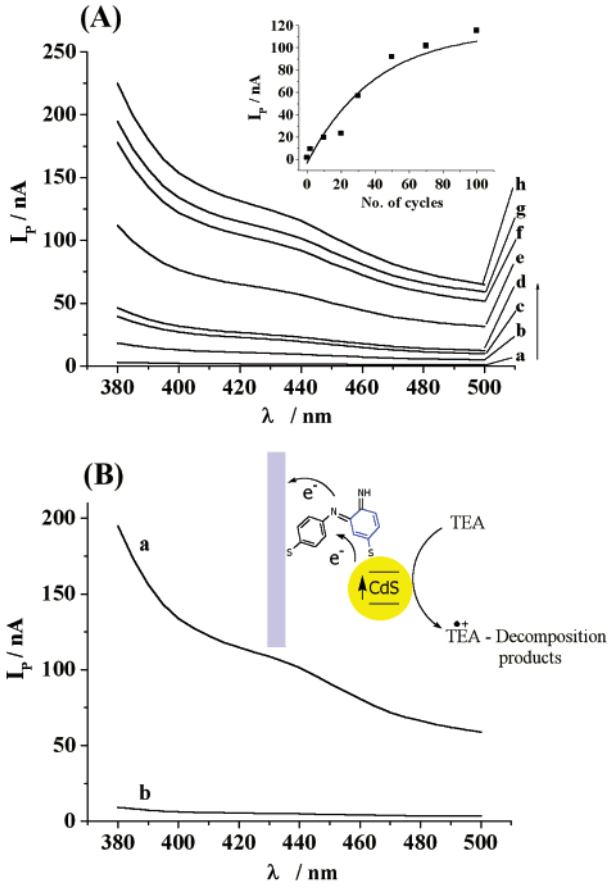

Figure 6. (A) Photocurrent action spectra of the CdS-nanoparticle-modified Au electrodes generated by a variable number of electrochemical deposition cycles: (a) *p*-ATP-functionalized electrode; (b−h) electrodes generated by 2, 10, 20, 30, 50, 70, and 100 electrochemical cycles, respectively. Inset: Photocurrent values at 440 nm for the different electrodes that include variable surface coverages of the nanoparticles. (B) Photocurrents corresponding to (a) the CdS-modified electrode generated by the application of 70 electrochemical deposition cycles in the presence of CdS nanoparticles and (b) the *p*-ATP-monolayer-functionalized electrode after electropolymerization of 70 cycles in the absence of CdS nanoparticles. Inset: Schematic photoinduced generation of the photocurrent by the CdS-nanoparticle-functionalized electrode and mediated electron transfer by the cross-linking units. Photocurrents were recorded in 0.1 M phosphate buffer, pH = 11.5, in the presence of 20 mM triethanolamine (TEA).

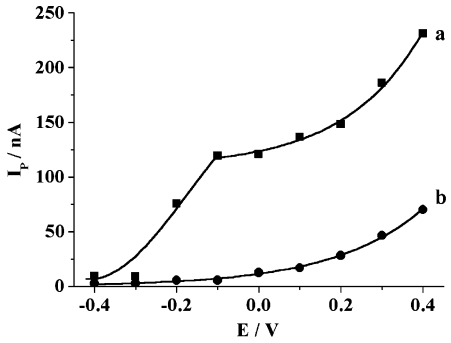

Figure 7. Photocurrent values at $\lambda = 440$ nm corresponding to: (a) The CdS-nanoparticle-functionalized electrode (generated by 100 electrochemical cycles) upon the application of different potentials on the electrode. (b) The cystamine/mercaptoethane sulfonic acid-functionalized CdS nanoparticles covalently linked to a Au electrode.

in the latter system reveals only a single monotonic region, where the photocurrent of the system is blocked upon biasing the potential to values that are negative to −0.10 V. (ii) The maximum photocurrent extracted in the reference cysteic acid−cystamine−CdS nanoparticle is 66 nA. Thus, the photocurrent observed in the present bisaniline cross-linked CdS nanoparticle system is substantially higher, as compared to the reference system. At an applied potential of 0.40 V the photocurrent is 230 nA, a value that is 3.5-fold higher than the photocurrent in the reference system ($\phi = 5.7\%$). At an applied potential of −0.20 V the observed photocurrent corresponds to 77 nA ($\phi = 1.9\%$), a value that is about 15-fold higher than the photocurrent in the reference system. These results clearly indicate that the electrochemical cross-linking of the *p*-ATP-capped CdS nanoparticle array yields a matrix with charge transport properties (mediated electron transport or tunneling transport according to the applied potential). The charge transport properties of the cross-linking matrix facilitate the charge separation in the system, retard the recombination process, and thereby enhance the resulting photocurrents.

Conclusions

The present study has introduced a new method to assemble functional nanoparticle arrays on surfaces by the electrochemically induced cross-linking of *p*-aminothiophenol-capped CdS nanoparticles to a *p*-aminothiophenol monolayer linked to a Au electrode. The different methods that were applied to characterize the system have revealed that the CdS nanoparticles form a densely packed monolayer on the surface. The resulting CdS nanoparticle array represents not only a new method for the assembly of nanoparticle architectures on surfaces, but the system reveals improved photoelectrochemical functionalities that originate from the charged transport properties of the molecular cross-linker. Specifically, the mediated electron transport of the conduction-band electrons by the oxidized dianiline cross-linker facilitates charge separation and leads to the enhanced generation of photocurrent.

As far as we are aware, this is the first example for the electrochemically induced assembly of semiconductor nanoparticles on electrodes. In contrast to previous methods that utilized the self-assembly of the particles by a layer-by-layer deposition processes, or the covalent attachment of the nanoparticles to monolayer-modified electrodes, the present method enables the continuous covalent binding of the nanoparticles to the electrode and the parallel monitoring of the binding process by electrochemical means. Besides the advantages of the method in tailoring homogeneous densely packed nanoparticle monolayers on the electrode, we reveal unprecedented functions of the redox-active cross-linking dianiline units in transporting the electrons from the semiconductor nanoparticles to the electrode. We believe that this method, and the beneficial electronic properties of the resulting electrodes, could be applied to tailor systems consisting of other nanoparticles.

Acknowledgment. This research (No. 101/00) is supported by the Israel Science Foundation.

References and Notes

(1) (a) Hicks, J. F.; Miles, D. T.; Murray, R. W. *J. Am. Chem Soc.* **2002**, *124*, 13322−13328. (b) Chen, S.; Ingram, R. S.; Hostetler, M. J.; Pietron, J. J.; Murray, R. W.; Schaaff, T. G.; Khoury, J. T.; Alvarez, M. M.; Whetten, R. L. *Science* **1998**, *280*, 2098−2101. (c) Lee, D.; Donkers, R. L.; DeSimone, J. M.; Murray, R. W. *J. Am. Chem. Soc.* **2003**, *125*, 1182−1183.

(2) (a) Alvarez, M. M.; Khoury, J. T.; Schaaff, T. G.; Shafigullin, M. N.; Vezmar, I.; Whetten, R. L. *J. Phys. Chem. B* **1997**, *101*, 3706−3712. (b) Alivisatos, A. P. *J. Phys. Chem.* **1996**, *100*, 13226−13239. (c) Kuczynski, J. P.; Milosavljevic, B. H.; Thomas, J. K. *J. Phys. Chem.* **1984**, *88*, 980−984.

(3) (a) Kesavan, V.; Sivanand, P. S.; Chandrasekaran, S.; Koltypin, Y.; Gedanken, A. *Angew. Chem., Int. Ed.* **1999**, *38*, 3521−3523. (b) Lewis, L. N. *Chem. Rev.* **1993**, *93*, 2693−2730. (c) Weizmann, Y.; Patolsky, F.; Willner, I. *Analyst* **2001**, *126*, 1502−1504.

(4) (a) Klein, D. L.; Roth, R.; Lim, A. K. L.; Alivisatos, A. P.; McEuen, P. L. *Nature* **1997**, *389*, 699−701. (b) Sato, T.; Ahmed, H.; Brown, D.; Johnson, B. F. G. *J. Appl. Phys.* **1997**, *82*, 696−701. (c) Feldheim, D. L.; Keating, C. D. *Chem. Soc. Rev.* **1998**, *27*, 1−12.

(5) (a) Sato, T.; Ahmed, H. *Appl. Phys. Lett.* **1997**, *70*, 2759−2761. (b) Weller, H. *Angew. Chem., Int. Ed.* **1998**, *37*, 1658−1659.

(6) (a) Shipway, A. N.; Katz, E.; Willner, I. *ChemPhysChem* **2000**, *1*, 18−52. (b) Shipway, A. N.; Willner, I. *Chem. Commun.* **2001**, 2035−2045.

(7) (a) Bandyopadhyay, K.; Patil, V.; Vijayamohanan, K.; Sastry, M. *Langmuir* **1997**, *13*, 5244−5248. (b) Colvin, V. L.; Goldstein, A. N.; Alivisatos, A. P. *J. Am. Chem. Soc.* **1992**, *114*, 5221−5230. (c) Baum, T.; Bethell, M.; Brust, M.; Schiffrin, D. J. *Langmuir* **1999**, *15*, 866−871.

(8) (a) Shipway, A. N.; Lahav, M.; Blonder, R.; Willner, I. *Chem. Mater.* **1999**, *11*, 13−15. (b) Schmitt, J.; Decher, G.; Dressick, W. J.; Brandow, S. L.; Geer, R. E.; Shashidhar, R.; Calvert, M. *Adv. Mater.* **1997**, *9*, 61−65. (c) Kotov, N. A.; Dekany, I.; Fendler, J. H. *J. Phys. Chem.* **1995**, *99*, 13065−13069. (d) Ariga, K.; Lvov, Y.; Onda, M.; Ichinose, I.; Kunitake, T. *Chem. Lett.* **1997**, 125−126.

(9) (a) Sarathy, K. V.; Thomas, P. J.; Kulkarni, G. U.; Rao, C. N. R. *J. Phys. Chem. B* **1999**, *103*, 399−401. (b) Li, M.; Wong, K. K. W.; Mann, S. *Chem. Mater.* **1999**, *11*, 23−26. (c) Brust, M.; Etchenique, R.; Calvo, E. J.; Gordillo, G. J. *Chem. Commun.* **1996**, 1949−1950.

(10) (a) Blonder, R.; Sheeney, L.; Willner, I. *Chem. Commun.* **1998**, 1393−1394. (b) Lahav, M.; Gabriel, T.; Shipway, A. N.; Willner, I. *J. Am. Chem. Soc.* **1999**, *121*, 258−259. (c) Lahav, M.; Gabai, R.; Shipway, A. N.; Willner, I. *Chem. Commun.* **1999**, 1937−1938.

(11) (a) Lvov, Y. M.; Rusling, J. F.; Thomsen, D. L.; Papadimitrakopoulos, F.; Kawakani, T.; Kunitake, T. *Chem. Commun.* **1998**, 1229−1230. (b) Cassagneau, T.; Fendler, J. H. *J. Phys. Chem. B* **1999**, *103*, 1789−1793. (c) Kovtyukhova, N. I.; Olliver, P. J.; Martin, B. R.; Mallouk, T. E.; Chizhik, S. A.; Buzaneva, E. V.; Gorchinskiy, A. D. *Chem. Mater.* **1999**, *11*, 771−778.

(12) (a) Patolsky, F.; Gabriel, T.; Willner, I. *J. Electroanal. Chem.* **1999**, *479*, 69−73. (b) Shipway, A. N.; Lahav, M.; Willner, I. *Adv. Mater.* **2000**, *12*, 993−998.

(13) (a) Patolsky, F.; Ranjit, K. T.; Lichtenstein, A.; Willner, I. *Chem. Commun.* **2000**, 1025−1026. (b) Willner, I.; Patolsky, F.; Wasserman, J. *Angew. Chem., Int. Ed.* **2001**, *40*, 1861−1864.

(14) (a) Pardo-Yissar, V.; Gabai, R.; Shipway, A. N.; Bourenko, T.; Willner, I. *Adv. Mater.* **2001**, *13*, 1320−1323. (b) Pardo-Yissar, V.; Bourenko, T.; Wasserman, J.; Willner, I. *Adv. Mater.* **2002**, *14*, 670−673. (c) Sheeney-Haj-Ichia, L.; Sharabi, G.; Willner, I. *Adv. Funct. Mater.* **2002**, *12*, 27−32.

(15) Hata, K.; Fujihara, H. *Chem. Commun.* **2002**, 2714−2715.

(16) (a) Hagfeldt, A.; Grätzel, M. *Chem. Rev.* **1995**, *95*, 49−68. (b) Kamat, P. V. *Chem. Rev.* **1993**, *93*, 267−300.

(17) Cassagneau, T.; Mallouk, T. E.; Fendler, J. H. *J. Am. Chem. Soc.* **1998**, *120*, 7847−7859.

(18) (a) Kumar, N. D.; Joshi, M. P.; Friend, C. S.; Prasad, P. N. *Appl. Phys. Lett.* **1997**, *71*, 1388−1390. (b) Colvin, V. L.; Schlamp, M. C.; Alivisatos, A. P. *Nature* **1994**, *370*, 354−357. (c) Dabbousi, B. O.; Bawendi, M. G.; Onitsuka, O.; Rubner, M. F. *Appl. Phys. Lett.* **1995**, *66*, 1316−1318.

(19) (a) O'Regan, B.; Grätzel, M. *Nature*, **1991**, *353*, 737−739. (b) Burnside, S. D.; Shklover, V.; Barbe, C.; Comte, P.; Arendse, F.; Brooks, K.; Grätzel, M. *Chem. Mater.* **1998**, *10*, 2419−2425.

(20) (a) Imahori, H.; Fukuzumi, S. *Adv. Mater.* **2001**, *3*, 1197−1199. (b) Imahori, H.; Tanaki, K.; Araki, Y.; Hasobe, T.; Ito, O.; Shimomura, A.; Kundu, S.; Okada, T.; Sakata, Y.; Fukuzumi, S. *J. Phys. Chem. A* **2002**, *106*, 2803−2814. (c) Yanada, H.; Imahori, H.; Nishimura, Y.; Yamazaki, I.; Fukuzumi, S. *Adv. Mater.* **2002**, *14*, 892−895.

(21) (a) Nasr, C.; Hotchandani, S.; Kim, W. Y.; Schmehl, R. H.; Kamat, P. V. *J. Phys. Chem. B* **1997**, *101*, 7480−7487. (b) Gopidas, K. R.; Bohorquez, M.; Kamat, P. V. *J. Phys. Chem.* **1990**, *94*, 6435−6440. (c) Liu, D.; Kamat, P. V. *J. Phys. Chem.* **1993**, *97*, 10769−10773.

(22) Zaban, A.; Chen, S. G.; Chappel, S.; Gregg, B. A. *Chem. Commun.* **2000**, 2231−2232.

(23) Miyake, M.; Matsaumoto, H.; Nishizawa, M.; Sakata, T.; Mori, H.; Kuwabata, S.; Yoneyama, H. *Langmuir* **1997**, *13*, 742−746.

(24) (a) Haram, S. K.; Quinn, B. M.; Bard, A. J. *J. Am. Chem. Soc.* **2001**, *123*, 8860−8861. (b) Sheeney-Haj-Ichia, L.; Wasserman, J.; Willner, I. *Adv. Mater.* **2002**, *14*, 1323−1326.

(25) Lukkari, J.; Kleemola, K.; Meretoja, M.; Ollonqvist, T.; Kankare, J. *Langmuir* **1998**, *14*, 1705−1715.

(26) (a) Barlett, P. N.; Wang, J. H. *J. Chem. Soc., Faraday Trans.* **1996**, *92*, 4137−4143. (b) Barlett, P. N.; Birkin, P. R.; Wallace, E. N. K. *J. Chem. Soc., Faraday Trans.* **1997**, *93*, 1951−1960.

(27) (a) Bartlett, P. N.; Simon, E. *Phys. Chem. Chem. Phys.* **2000**, *2*, 2599−2606. (b) Raitman, O. A.; Katz, E.; Bückmann, A. F.; Willner, I. *J. Am. Chem. Soc.* **2002**, *124*, 6487−6496.

(28) Xiao, Y.; Kharitonov, A. B.; Patolsky, F.; Weizmann, Y.; Willner, I. *Chem. Commun.* **2003**, 1540−1541.

(29) Bourdillon, C.; Demaille, C.; Gueris, J.; Moiroux, J.; Savéant, J. M. *J. Am. Chem. Soc.* **1993**, *115*, 12264−12269.